



Australian Journal of Earth Sciences

An International Geoscience Journal of the Geological Society of Australia


ISSN: (Print) (Online) Journal homepage: www.tandfonline.com/journals/taje20


Geodynamic evolution in the post-collisional stage of the East Kunlun Orogenic Belt: constraints from the Late Triassic intermediate–felsic igneous rocks

A-K. Zhang, S-Y. He, Y. Zhang, J-L. Sun & Y. Qian


To cite this article: A-K. Zhang, S-Y. He, Y. Zhang, J-L. Sun & Y. Qian (2024) Geodynamic evolution in the post-collisional stage of the East Kunlun Orogenic Belt: constraints from the Late Triassic intermediate–felsic igneous rocks, Australian Journal of Earth Sciences, 71:1, 114-128, DOI: [10.1080/08120099.2023.2263883](https://doi.org/10.1080/08120099.2023.2263883)

To link to this article: <https://doi.org/10.1080/08120099.2023.2263883>

 View supplementary material 

 Published online: 23 Oct 2023.

 Submit your article to this journal 

 Article views: 73

 View related articles 

 View Crossmark data 

Geodynamic evolution in the post-collisional stage of the East Kunlun Orogenic Belt: constraints from the Late Triassic intermediate–felsic igneous rocks

A-K. Zhang^a, S-Y. He^a, Y. Zhang^a, J-L. Sun^{b,c} and Y. Qian^{b,d}

^aThe Third Geological Exploration Institute of Qinghai Province, Xi'ning, China; ^bCollege of Earth Sciences, Jilin University, Changchun, China; ^cState Key Laboratory of Ore Deposit Geochemistry, Institute of Geochemistry, Chinese Academy of Sciences, Guiyang, China; ^dShandong Provincial Engineering Laboratory of Application and Development of Big Data for Deep Gold Exploration, Weihai, China

ABSTRACT

The Late Triassic igneous rocks associated with post-collision are widely distributed in the East Kunlun Orogenic Belt (EKOB), but their specific dynamic mechanism and evolutionary process are still controversial. To address these key issues, we investigated the geochronology and geochemistry of intermediate–felsic igneous rocks from the EKOB, including trachyandesite, rhyolite, porphyritic monzogranite, syenogranite, granite porphyry and crystalline tuff. Zircon U–Pb isotopes of these rocks indicate that they were formed between 231.1 and 215.8 Ma (*i.e.* Late Triassic). These igneous rocks have moderate to high SiO₂ (60.29–79.56 wt%) and low mantle compatible element contents (*e.g.* Co: 0.37–12.62 ppm; Ni: 1.55–15.59 ppm), suggesting that continental crustal-derived material played an important role in their formation. Porphyritic monzogranite (231.1 Ma), syenogranite (228.1 Ma), trachyandesite (227.4 Ma) and rhyolite (215.8 Ma) have Nb/U (1.41–4.71) and Ce/Pb (1.48–6.19) ratios like that of the crust, with $\epsilon\text{Hf}(t)$ values (–1.31 to 2.26) and old two-stage model ($T_{\text{DM}2}$) ages of 1340–1119 Ma, suggesting that they originated from the partial melting of a Mesoproterozoic crust with minor mantle material involved in their source. Crystalline tuff (224.6 Ma) and granite porphyry (222.3 Ma) have Nb/U (1.93–3.81) and Ce/Pb (0.30–3.18) ratios, negative $\epsilon\text{Hf}(t)$ values (–7.04 to –5.12) and old $T_{\text{DM}2}$ ages (1703–1581 Ma) closer to those of crust, suggesting that they were derived from the partial melting of a Paleo–Mesoproterozoic continental crust without addition of mantle material. Based on our new data and published data, the Late Triassic igneous rocks from the EKOB can be divided into three stages, 236–227, 226–218 and 216–208 Ma, corresponding to slab break-off, lithospheric mantle delamination and thickened lower crust delamination, respectively.

KEY POINTS

1. The intermediate–felsic igneous rocks from the East Kunlun Orogenic Belt are dated from 231.1 to 215.8 Ma (*i.e.* Late Triassic).
2. These igneous rocks were derived from the partial melting of ancient continental crust.
3. The Late Triassic igneous rocks from the East Kunlun Orogenic Belt can be divided into three stages, including slab break-off, lithospheric mantle delamination and thickened lower crust delamination.

ARTICLE HISTORY

Received 26 June 2023
Accepted 23 September 2023

KEYWORDS

East Kunlun Orogenic Belt; Late Triassic; post-collisional magmatism; geodynamic evolution; intermediate–felsic igneous rocks; slab break-off; delamination

Introduction

The East Kunlun Orogenic Belt (EKOB) is a typical collisional orogenic belt in the north of the Tibetan Plateau (Figure 1a; Sun *et al.*, 2009; Windley *et al.*, 2007; Xiao *et al.*, 2009). It not only records the earliest accretion history of the Gondwana and Laurasia supercontinent (Roger *et al.*, 2003; Yin & Harrison, 2000), but also completely preserves the evolution of Proto-Tethys Ocean before the early Paleozoic, and the Paleo-Tethys Ocean from the Paleozoic to Mesozoic (Mo *et al.*, 2007; Roger *et al.*, 2003; Sengör, 1979; Sun *et al.*,

2009, 2021; Xiong, 2014). The evolutionary process of the Paleo-Tethys Ocean controlled the present-day geological structure of the EKOB. The opening of the Paleo-Tethys Ocean took place in the Late Devonian to Carboniferous (Mo *et al.*, 2007), and initial subduction began in the Early Permian (Chen *et al.*, 2001; Liu *et al.*, 2014; Xiong, 2014). Rocks associated with the collision appeared in the Early–Middle Triassic (Hu *et al.*, 2016; Li *et al.*, 2018; Xiong *et al.*, 2014). Most scholars proposed that the EKOB had entered the post-collisional stage in the Late Triassic (Sun *et al.*, 2021;

CONTACT Ye Qian ✉ qianye@jlu.edu.cn; Jin-Lei Sun ✉ jinleisun123@163.com College of Earth Sciences, Jilin University, No. 2199, Jianshe Street, Changchun 130061, China

Supplemental data for this article can be accessed online at <https://doi.org/10.1080/08120099.2023.2263883>.

Editorial handling: Chris Fergusson

© 2023 Geological Society of Australia

Xiong *et al.*, 2012, 2014; Yu *et al.*, 2015; Zhao *et al.*, 2020). However, Ding *et al.* (2014) reported that the Anisian granite dykes (*ca* 244 Ma) had the characteristics of A₂-type granites and suggested that the EKOB entered the post-collisional stage prior to the Middle Triassic. In addition, the specific dynamic mechanism and evolutionary process of the post-collisional stage are still controversial, and several dynamic models have been proposed, such as slab break-off (Luo *et al.*, 2014; Xia, Wang, *et al.*, 2014) and delamination of thickened lithospheric mantle (Xiong *et al.*, 2014; Zhou *et al.*, 2021), whereas no model can explain fully the petrogenesis and rock assemblages of the Late Triassic in the EKOB.

Intermediate-felsic igneous rocks are the most important rock types in orogenic belts and are widely distributed in various evolutionary stages of orogenic belts. Their spatial-temporal distribution records fully the timelines and processes of dynamic evolution, such as subduction, collision, post-collision, slab break-off and lithospheric delamination (Bellos *et al.*, 2015; Xia, Wang, *et al.*, 2014; Xin *et al.*, 2019). Therefore, a systematic summary of the types and genesis of intermediate-felsic igneous rocks can provide constraints on the dynamic mechanism and evolutionary process. During the Late Triassic, numerous intermediate-felsic igneous rocks associated with post-collision occurred in the EKOB (Figure 1b). In this study, samples of the Late Triassic intermediate-felsic igneous rocks from the Yazigou and Harizha areas of the EKOB have been collected, and experiments undertaken on geochemistry, zircon U–Pb geochronology and Hf isotopes. We analysed their petrogenesis and tectonic setting, and summarised the rock assemblages and their distribution, with the aim of providing a new insight into the post-collisional stage of the Paleo-Tethys Ocean in the EKOB.

Geological setting and sample descriptions

The EKOB is in the north Tibetan Plateau, bounded by the Qaidam Block to the north, the Bayan Har–Songpanganzi Terrane (BH-SG) to the south, and the Tarim block to the west (Figure 1a). The EKOB is more than 1500 km long in

an east–west direction and about 50–200 km wide, and divided into three tectonic belts (NKB, North Kunlun Belt; CKB, Central Kunlun Belt; SKB, South Kunlun Belt) by three faults (NKF, North Kunlun fault; CKF, Central Kunlun fault; SKF, South Kunlun fault; Figure 1b; Sun *et al.*, 2009).

The Precambrian basement is mainly the Paleoproterozoic Jinshuikou Group in the NKB and CKB. The Jinshuikou Group contains moderate–high metamorphic rocks, comprising the Baishahe and Xiaomiao formations (Chen *et al.*, 2006; Wang *et al.*, 2007). The Precambrian strata in the SKB consist mainly of the Proterozoic Kukai Group and Meso–Neoproterozoic Wanbaogou Group (Xiong, 2014). The Kukai Group consists of greenschist to amphibolite metamorphic rocks, and the Wanbaogou Group is a very thick volcano–sedimentary unit. Permian and Triassic strata in the SKB include the Buqingshan Group, and the Gequ, Hongshuichuan, Naocanjiangou and Xilikete formations. Note that the Middle Triassic Naocanjiangou Formation is angularly unconformably overlain by the Middle Triassic Xilikete Formation (Chen, 2014).

The igneous rocks are mainly distributed in the CKB with minor occurrences in the NKB and SKB (Figure 1b). These rocks were mainly formed from the late Paleozoic to Mesozoic, especially the Late Permian to Late Triassic (Chen *et al.*, 2019; Mo *et al.*, 2007). Intrusive rocks include mafic rocks, diorites, granites and parts of ophiolitic complexes. Granites are the most extensive with an area of 48 000 km² in large complex batholiths (Figure 1b; Liu *et al.*, 2011; Sun *et al.*, 2021; Xin *et al.*, 2019; Xiong *et al.*, 2011, 2012, 2014). Granites contain mafic microgranular enclaves (MMEs, Xiong, 2014). In addition, the Devonian Maoniushan Formation and Late Triassic Elashan Formation, which are composed of continental volcanic rocks, occur in the region. The Elashan Formation consists of lower volcanic lava (basalt, andesite and rhyolite) and upper volcanoclastic rocks (crystalline tuff) (Ding *et al.*, 2011).

The study areas are in the Yazigou area of the NKB and the Harizha area of the CKB (Figures 1b and 2). Exposed strata are mainly the Jinshuikou Group, Ordovician–Silurian Najitai Group, Permian Dachaigou Formation and Late Triassic Elashan Formation. The Najitai Group consists of

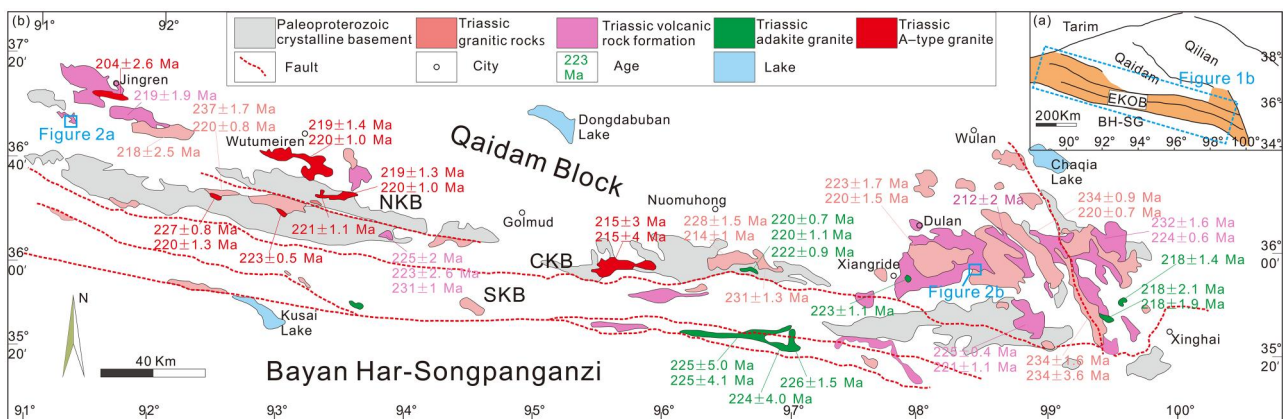


Figure 1. (a) Tectonic map of China (after Yuan *et al.*, 2010). (b) Schematic geological map of the East Kunlun Orogen Belt (after Fan *et al.*, 2022). NKB, North Kunlun Belt; CKB, Central Kunlun Belt; SKB, South Kunlun Belt. The geochronological data are listed in the Supplemental data (Table S4).

typical volcano-sedimentary assemblages, which are divided into three parts: (1) phyllite with marble interlayers in the lower part; (2) phyllite, dacite and slate in the middle part; and (3) altered basalt and tuff in the upper part. The Dachaigou Formation comprises mainly marble and limestone. The Elashan Formation comprises mainly tuff and rhyolite. In addition, numerous igneous rocks occur in the study areas and include andesite, rhyolite, tuffaceous rocks and granite (Figure 2). In this study, six representative samples of intermediate-felsic igneous rocks were collected, including porphyritic monzogranite (YZG-N1), syenogranite (YZG-N2), trachyandesite (YZG-N3), rhyolite (YZG-N4), granite porphyry (HRZ-N4) and crystalline tuff (HRZ-54) (Figure 2). Except for the syenogranite, all other samples have a porphyritic structure (Figure 3). The porphyritic monzogranite has phenocrysts (40 vol%) and matrix (60 vol%) of K-feldspar, plagioclase, quartz, with minor biotite and amphibole. The syenogranite comprises K-feldspar (60 vol%), quartz (20–25 vol%), plagioclase (~10 vol%) and minor biotite (<5 vol%). The trachyandesite has phenocrysts (~30 vol%) and matrix (70 vol%) of quartz, K-feldspar, plagioclase, amphibole and biotite. The rhyolite exhibits phenocrysts (~25 vol%) and matrix (~75 vol%) of plagioclase and quartz, in which plagioclase is altered by sericite. The granite porphyry has phenocrysts (~30 vol%) and matrix (70 vol%) of K-feldspar, plagioclase and quartz. The crystalline tuff has phenocrysts (25–30 vol%) and matrix (60–75 vol%) of K-feldspar, plagioclase, quartz and biotite.

Analytical methods

Zircon U–Pb dating and major- and trace-element analyses were carried out at the Key Laboratory of Mineral Resources Evaluation in Northeast Asia, Ministry of Nature Resources of China, Changchun.

Zircon U–Pb dating

Zircons were separated from the six samples by magnetic and heavy-liquid separation techniques at Langfang Regional Geological Survey, Hebei Province, China. These zircons were imaged in transmitted light and cathodoluminescence to reveal their internal morphology. The zircon U–Pb analyses were determined by Agilent 7900 ICP-MS with a 193 nm ArF excimer laser system. The beam diameter was 32 μm , with a frequency of 8 Hz and energy density of 10 J/cm² during the analyses. The zircon standards 91500 and GJ were adopted for age calibration, and NIST610 silicate glass was used to quantify the element concentration. During the analyses, the zircon standard 91500 showed an average age of 1064.90 Ma, which is consistent with the recommended age values of 1065.4 \pm 0.6 Ma (Wiedenbeck *et al.*, 1995). Details of the method are given by Liu *et al.* (2008). The ICP-MS DataCal 10.8 (Liu *et al.*, 2008) and Isoplot3 program (Ludwig, 2003) were used to plot age and concordia plots. Common Pb corrections followed the method of Andersen (2002). Zircon U–Pb age data are listed in the Supplemental data (Table S1).

Major- and trace-element analyses

Thirty-four samples for major and trace elements were tested by X-ray fluorescence (XRF; ZXS Primus II) and Agilent 7500a ICP-MS. After removing the weathered surfaces, samples were smashed to 200-mesh size. The sample powder and lithium borate flux were mixed, melted and cooled into glass discs for XRF testing. Sample powders were dissolved by acid (HF + HNO₃) in a Teflon bomb and dissolved into an aqueous solution for ICP-MS analysis. The accuracy of the samples was monitored using national standard GBW07103 and GBW07104. The precision is

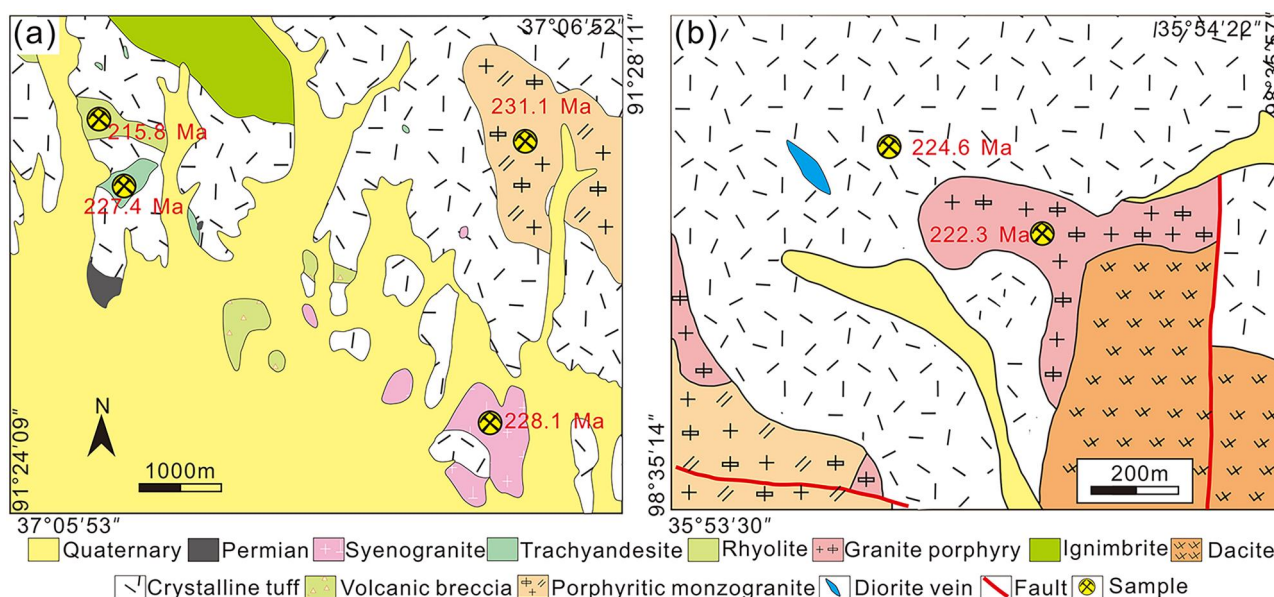


Figure 2. Detailed geological map of the Yazigou (a) and Harizha (b) areas with sample locations. Modified after 1:100 000 geological maps of Qinghai Provincial Bureau of Nonferrous Metal and Geological Exploration.

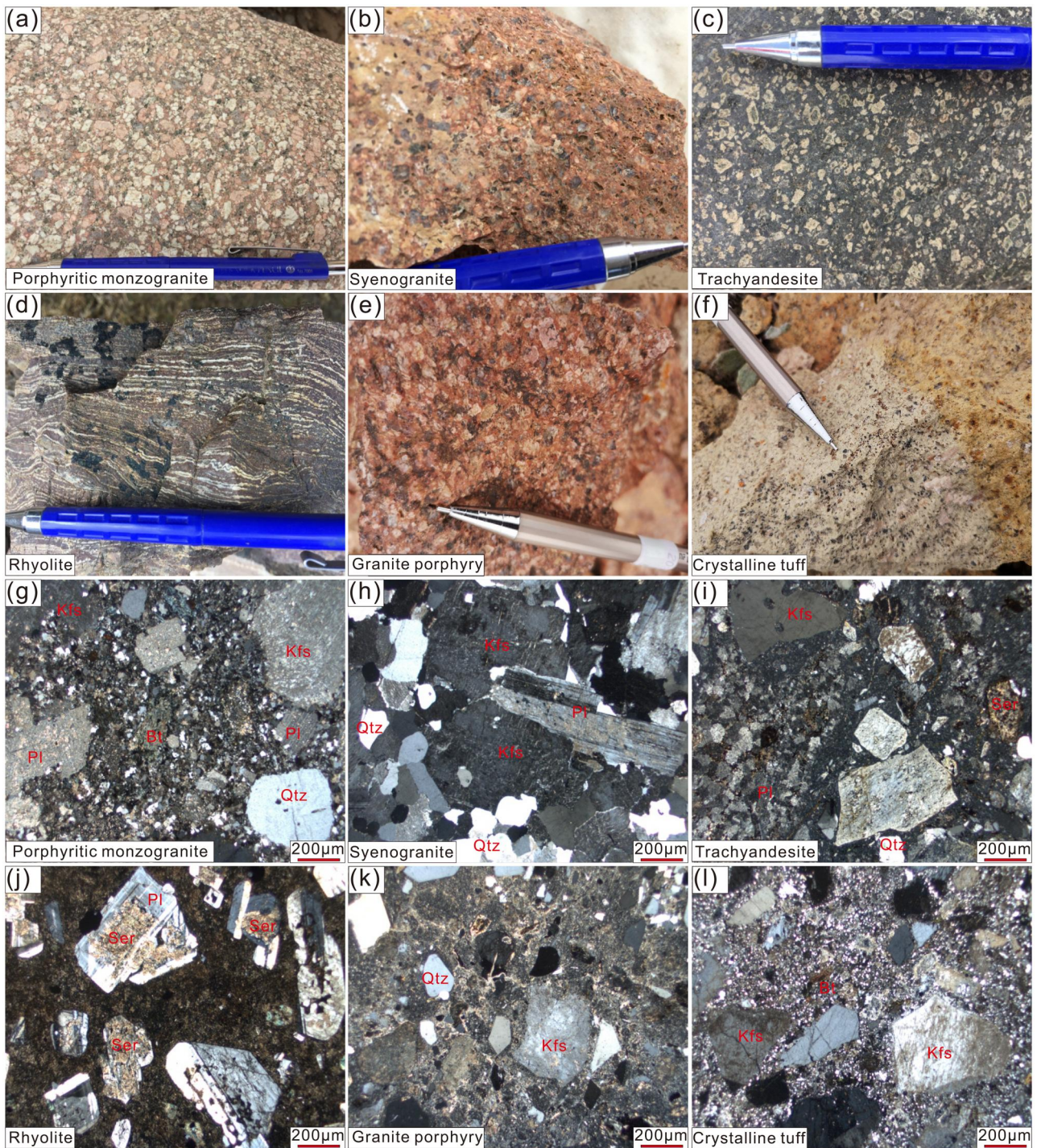


Figure 3. (a–f) Field photographs and photomicrographs showing typical texture features. (g–l) Cross-polarised light. (a, g) Porphyritic monzogranite, (b, h) syenogranite (c, i) trachyandesite, (d, j) rhyolite, (e, k) granite porphyry, and (f, l) crystalline tuff. Kfs, K-feldspar; Pl, plagioclase; Qtz, quartz; Bt, biotite; Ser, sericite.

$<\pm 5\%$ for major elements and $<\pm 10\%$ for trace elements. The major- and trace-element data are provided in the [Supplemental data](#) (Table S2).

Zircon Hf isotopic compositions

Zircon Hf isotopic analyses were completed by Neptune plus MC-ICP-MS with a 193 nm ArF excimer laser system at

the Institute of Mineral Resources, Chinese Academy of Geological Sciences, Beijing, China. Ablation protocol employed a spot diameter of 55 μm with an 8 Hz repetition rate and laser energy of 10 J/cm². The 91500 zircon standards were used for precision control. During the analyses, the 91500 zircon standards yielded a weighted-mean ¹⁷⁶Hf/¹⁷⁷Hf ratio of 0.282298, which is in good agreement with the recommended Hf isotopic ratio (¹⁷⁶Hf/¹⁷⁷Hf =

0.282302 ± 0.000008; Goolaerts *et al.*, 2004). Details of the calibration methods followed Wu *et al.* (2006). Zircon Hf isotopic compositions are listed in the [Supplemental data \(Table S3\)](#).

Results

Zircon U–Pb ages and Hf isotopic compositions

Zircons from the samples are mainly subhedral, with some being euhedral. Their length ranges from 50 to 100 µm, with an aspect ratio of 1–2. Zircons from samples YZG-N1, YZG-N3 and HRZ-N4 have obvious oscillatory growth zoning, whereas other zircons have only weak growth zoning. All zircons have high Th/U ratios (0.25–1.3) indicating an igneous origin (Hoskin & Schaltegger, 2003).

Twenty-six zircons from porphyritic monzogranite (YZG-N1) yielded $^{206}\text{Pb}/^{238}\text{U}$ ages between 234.9 and 227.6 Ma, with a weighted-mean age of 231.1 ± 0.92 Ma (MSWD = 0.83; [Figure 4a](#)) considered to be the crystallisation age of the porphyritic monzogranite. Ten zircons have $\varepsilon\text{Hf}(t)$ values of –0.93 to 1.45, Hf single-stage model ages (T_{DM1}) ages of 919–819 Ma and two-stage model (T_{DM2}) ages of 1324–1172 Ma ([Figure 5](#)).

Thirteen zircons from syenogranite (YZG-N2) showed $^{206}\text{Pb}/^{238}\text{U}$ ages ranging from 231.5 to 225.3 Ma, giving a weighted-mean age of 228.1 ± 1.3 Ma (MSWD = 0.66; [Figure 4b](#)), which is regarded as the emplacement age of the syenogranite. Ten zircons have $\varepsilon\text{Hf}(t)$ values of –1.24 to 2.26, T_{DM1} ages of 930–786 Ma and T_{DM2} ages of 1340–1119 Ma ([Figure 5](#)).

Twenty-one zircons from trachyandesite (YZG-N3) displayed $^{206}\text{Pb}/^{238}\text{U}$ ages that vary between 229.5 and 226.0 Ma, with a weighted-mean age of 227.4 ± 1.3 Ma (MSWD = 0.21; [Figure 4c](#)), representing the crystallisation age of the trachyandesite. Nine zircons have $\varepsilon\text{Hf}(t)$ values of –1.08 to 0.70, T_{DM1} ages of 912–866 Ma and T_{DM2} ages of 1330–1217 Ma ([Figure 5](#)).

Twenty zircons from rhyolite (YZG-N4) have $^{206}\text{Pb}/^{238}\text{U}$ ages from 218.7 to 212.5 Ma, with a weighted-mean age of 215.8 ± 0.94 Ma (MSWD = 0.63; [Figure 4d](#)), which can be taken as the crystallisation age of the rhyolite. Ten zircons have $\varepsilon\text{Hf}(t)$ values of –1.31 to 2.01, T_{DM1} ages of 928–794 Ma and T_{DM2} ages of 1332–1123 Ma ([Figure 5](#)).

Twenty-five zircons from granite porphyry (HRZ-N4) yielded $^{206}\text{Pb}/^{238}\text{U}$ ages ranging from 228.7 to 219.5 Ma, giving a weighted-mean age of 222.3 ± 0.94 Ma (MSWD = 0.44; [Figure 4e](#)), which is recorded as the crystallisation age of the granite porphyry. Nine zircons have $\varepsilon\text{Hf}(t)$ values of –7.04 to –5.12, T_{DM1} ages of 1151–1077 Ma and T_{DM2} ages of 1703–1581 Ma ([Figure 5](#)).

Seventeen zircons from crystalline tuff (HRZ-54) showed $^{206}\text{Pb}/^{238}\text{U}$ ages between 227.7 and 222.5 Ma, with a weighted-mean age of 224.6 ± 1.9 Ma (MSWD = 0.14; [Figure 4f](#)), which is interpreted to be the crystallisation age of the crystalline tuff.

Major and trace elements

Most of the samples have low loss in ignition (LOI) contents (0.39–2.81 wt%). All samples have moderate to high SiO_2 (60.29–79.56 wt%) and moderate Al_2O_3 (10.3–17.54 wt%) and total alkali ($\text{K}_2\text{O} + \text{Na}_2\text{O}$) contents (5.71–8.82 wt%). Except for the trachyandesite sample, the contents of CaO, MgO, P_2O_5 , TiO_2 and MnO from other samples are less than 2 wt%, and the $\text{Fe}_2\text{O}_3^{\text{T}}$ is less than 4 wt%. The trachyandesite samples have low–moderate MgO (1.89–2.11 wt%), CaO (3.46–4.25 wt%) and $\text{Fe}_2\text{O}_3^{\text{T}}$ contents (5.51–5.93 wt%). All samples show subalkaline and high-K to shoshonite features ([Figure 6](#)). The porphyritic monzogranites have positive Eu anomalies ($\text{Eu}/\text{Eu}^* = 1.23\text{--}1.67$), whereas other samples have negative Eu anomalies ($\text{Eu}/\text{Eu}^* = 0.12\text{--}0.87$). Except for the granite porphyry, other samples show obvious enrichment in light rare earth element (REE) and depletion in heavy REE, with high $(\text{La}/\text{Yb})_{\text{N}}$ ratios of 4.3–26 ([Figure 7](#)). These samples are marked by enrichment in Rb, K, U, Pb, Zr and Hf elements, and depletion of high-field-strength elements (HFSEs, *e.g.* Nb, Ta and Ti; [Figure 7](#)).

Discussion

Petrogenesis

Although the LOI of these samples is low (0.39–2.81 wt%), it is necessary to exclude the effect of alteration on the major and trace elements before using them to discuss the potential magma sources. Published studies have shown that large-ion lithophile elements (LILEs) migrate more readily in hydrothermal fluids than HFSEs, so some LILEs (*e.g.* K, Sr, Rb) can be used to monitor alteration effects (Alirezai & Cameron, 2002; Rudnick *et al.*, 1985). In the K_2O and Sr vs LOI diagrams ([Supplementary material, Figure S1a, b](#)), the relative stability of K_2O and Sr in these rocks indicates that LILEs do not change significantly during weak alteration. In addition, zirconium (Zr) in the magmatic rocks is immobile during alteration, so some HFSEs are plotted against Zr to determine their migration. The Nb and Ta display linear relationships or clumps with Zr ([Supplementary material, Figure S1c, d](#)), suggesting that the HFSEs were not affected by weak alteration. Thus, the major and trace elements can be used for the following magmatic source assessment.

Porphyritic monzogranite and syenogranite

Granitic rocks can generally be divided into four rock types (I-, S-, M- and A-type; Chappell, 1999; Eby, 1992). The 231–228 Ma porphyritic monzogranite and syenogranite from the Yazigou area have high SiO_2 contents (66.50–75.64 wt%) and low MgO (0.15–0.62 wt%), Co (1.91–5.12 ppm) and Ni (3.30–7.93 ppm) contents, suggesting they are not M-type granite. These samples have low zircon saturation temperatures (T_{Zr}) between 763 and 845 °C

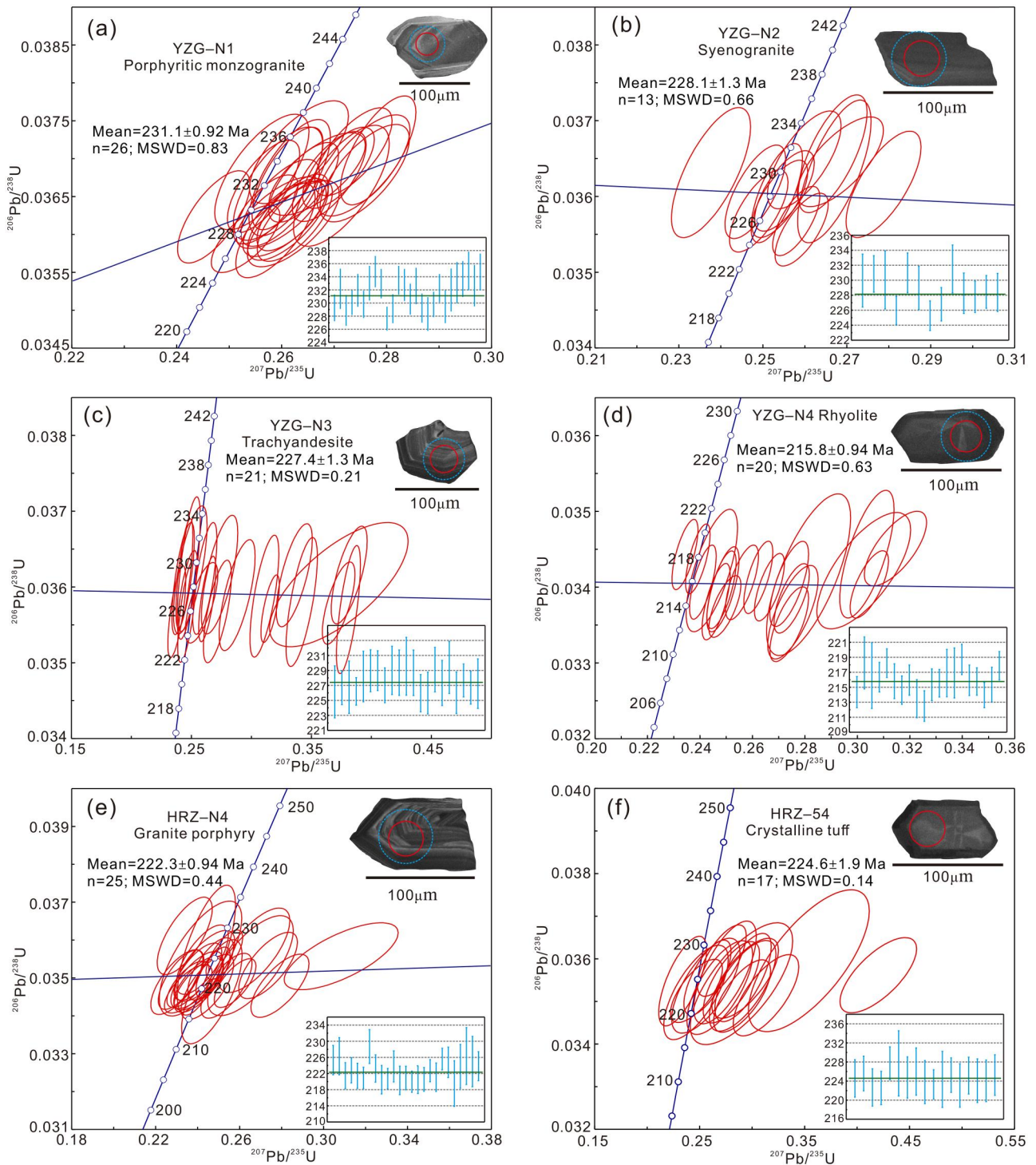


Figure 4. U–Pb concordia diagrams and weighted-mean age for zircons from the samples. Cyan dotted and red solid circles represent the locations of Hf isotope and U–Pb age.

(Watson & Harrison, 1983), and low Zr + Nb + Ce + Y values (162–348 ppm; only one sample is 375 ppm), which are not consistent with the features of A-type granite (>850 °C; >350 ppm). In the $\text{Fe}_2\text{O}_3/\text{MgO}$ and $(\text{K}_2\text{O} + \text{Na}_2\text{O})/\text{CaO}$ vs Zr + Nb + Ce + Y diagrams (Figure 8a, b; Whalen *et al.*, 1987), these samples plot in areas of non-A-type granite. In fact, these rocks show the characteristics of I-type granite.

They lack peraluminous minerals (*e.g.* cordierite and muscovite) and contain some amphibole and biotite (Figure 3). In addition, the negative correlation between P_2O_5 and SiO_2 also indicates that they belong to I-type granite.

I-type granite is thought to generated in three ways: fractional crystallisation of mantle-derived basaltic magmas (Chappell, 1999), partial melting of crustal materials

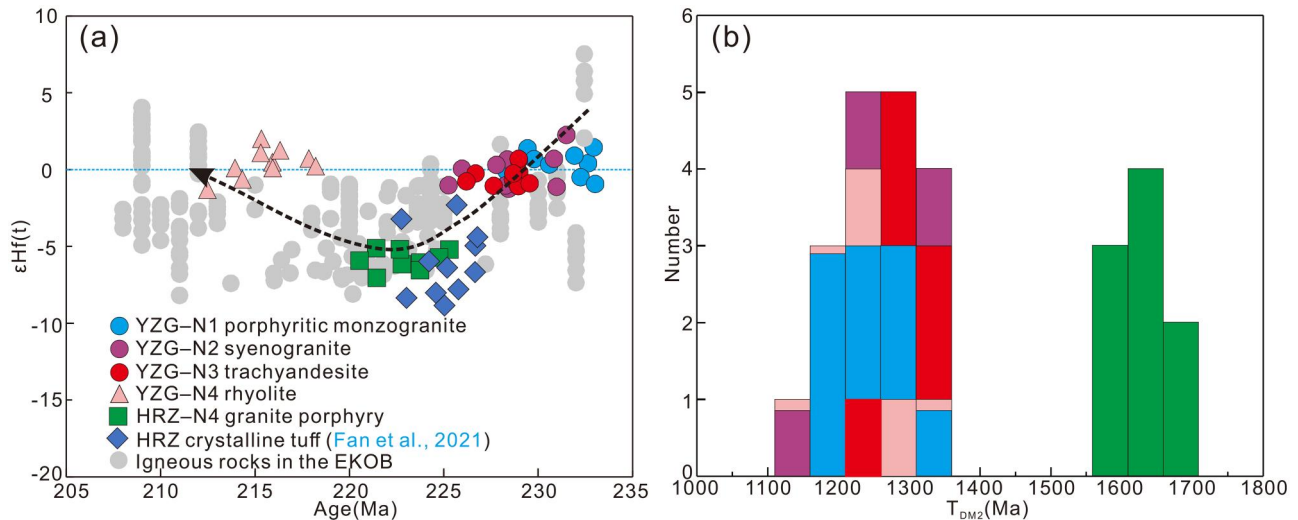


Figure 5. (a) $\epsilon\text{Hf}(t)$ vs age diagrams for zircon samples. (b) Histograms of T_{DM2} age for the zircons. The ϵHf isotope data for magmatic rocks in the EKOB are from Xiong *et al.* (2011, 2012, 2014) and Sun *et al.* (2021).

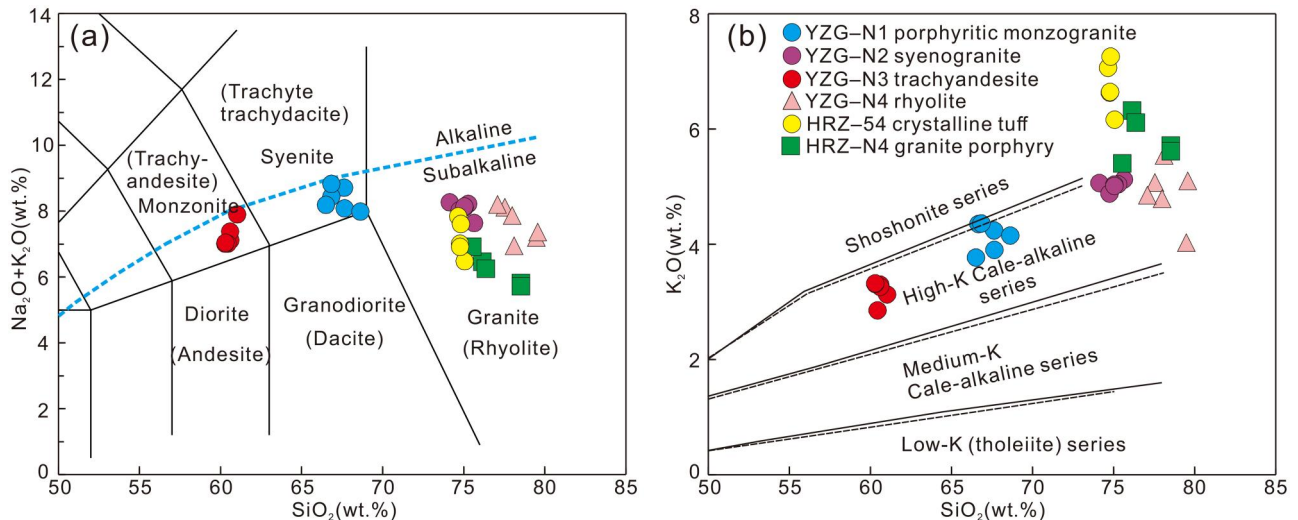


Figure 6. Major-element geochemical plots for samples from the Yazigou and Harizha areas in the EKOB: (a) total alkali vs SiO_2 (TAS) diagrams; (b) SiO_2 vs K_2O diagrams (Irvine & Baragar, 1971; Peccerillo & Taylor, 1976).

(Gao *et al.*, 2016; Richards, 2011) and mixing of crust- and mantle-derived magma (Champion & Chappell, 1992; Xie *et al.*, 2021). Fractional crystallisation of mantle-derived basaltic melts generally produces peralkaline magma, which is inconsistent with the calc-alkaline characteristics of these rocks (Figure 6a). High SiO_2 and low mantle compatible elements show also that mantle-derived magma was not obviously involved in their formation. Granitic rocks formed by mantle-derived magmatic differentiation are generally accompanied by many mafic and intermediate rocks in time and space (Turner *et al.*, 1992; Xin *et al.*, 2019), but this is not the case for rocks in the Yazigou area (Figure 2a, b). Their Nb/U (2.92–4.71) and Ce/Pb (1.48–6.19) ratios are closer to the crustal component (10 and 4) than to the mantle component (30 and 9) (Hofmann *et al.*, 1986), indicating that these samples have an affinity with continental crust. Their Rb/Sr (0.35–4.07) and Lu/Yb (0.16–0.19) ratios

are more consistent also with the partial melting of the crust (>0.5; 0.16–0.18) than those of the mantle (0.03–0.047; 0.14–0.15; Rudnick & Gao, 2003; Sun & McDonough, 1989). Porphyritic monzogranite and syenogranite have old T_{DM2} ages (1324–1172 Ma; 1340–1119 Ma), suggesting that they were formed by the partial melting of a Mesoproterozoic crust. In addition, their $\epsilon\text{Hf}(t)$ contents (–0.93 to 1.45; –1.24 to 2.26) indicate that only minor mantle material might have been added to their source.

Trachyandesite

Andesite is an important rock in orogenic belts, and its genetic study is significant for revealing crustal formation, growth and crust–mantle interaction (Chen & Zhao, 2017; Ji *et al.*, 2018). In general, andesites are formed in the following ways: (1) partial melting of mantle wedges that are

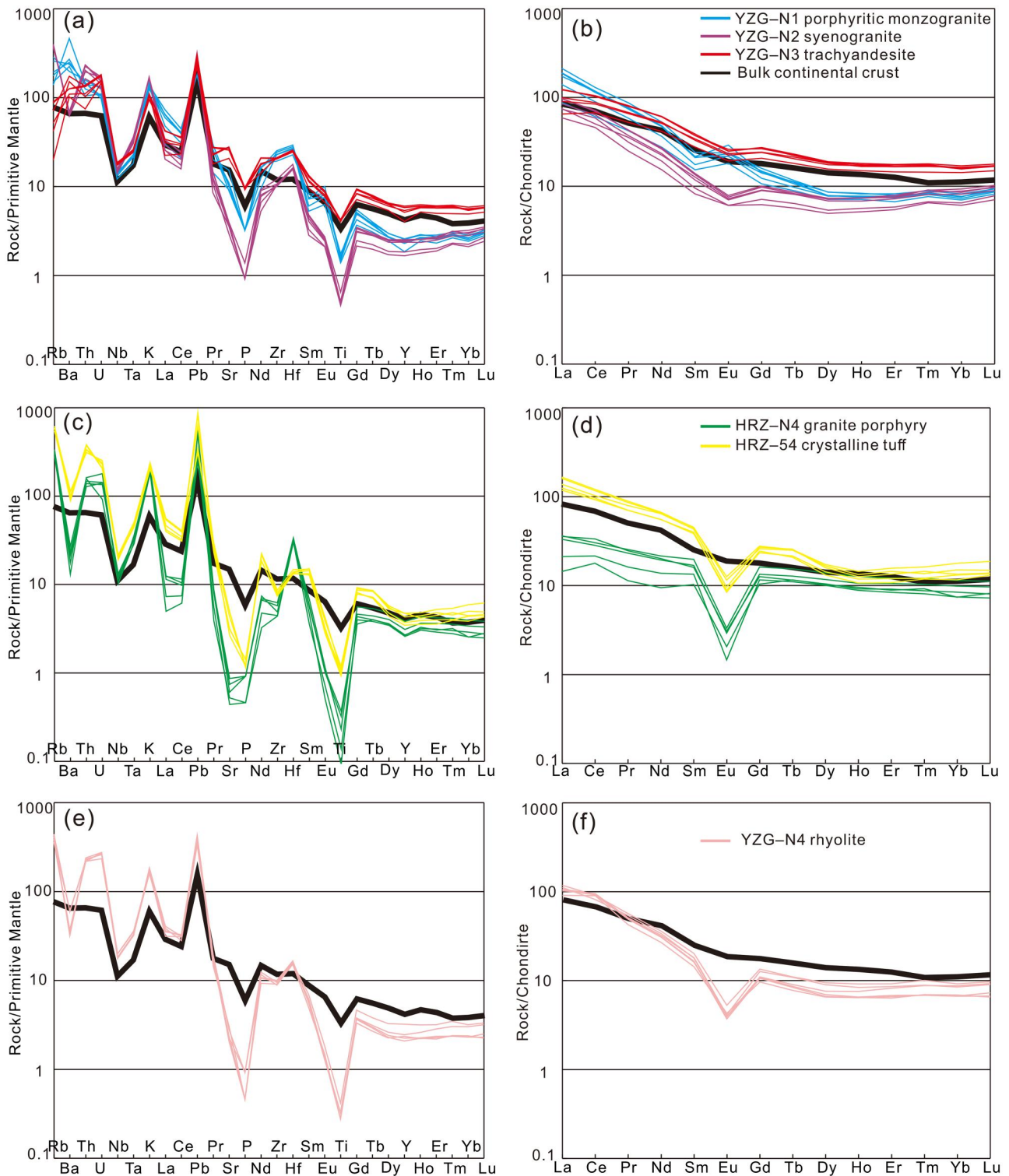


Figure 7. (a, c, e) Primitive mantle-normalised and (b, d, f) chondrite-normalised REE pattern trace-element diagrams for the samples (Boynton, 1984; Sun & McDonough, 1989). The model bulk continental crust is from Rudnick and Gao (2003).

metasomatised during subduction (Carmichael, 2002; Yu *et al.*, 2017), (2) assimilation and fractional crystallisation (AFC) of mantle-derived basaltic magma (Bonin, 2004; Lee *et al.*, 2014), (3) partial melting of the lower crust (Fliedert *et al.*, 2003; Guffanti *et al.*, 1996) and (4) mixing of crust-

derived felsic and mantle-derived basaltic magma (Guo *et al.*, 2007; Reubi & Blundy, 2009).

Partial melting of the mantle wedge will produce a rock with a high Mg# value (>60) and high Sr/Y ratio (Ji *et al.*, 2018; Xin *et al.*, 2019), which are not consistent with the low

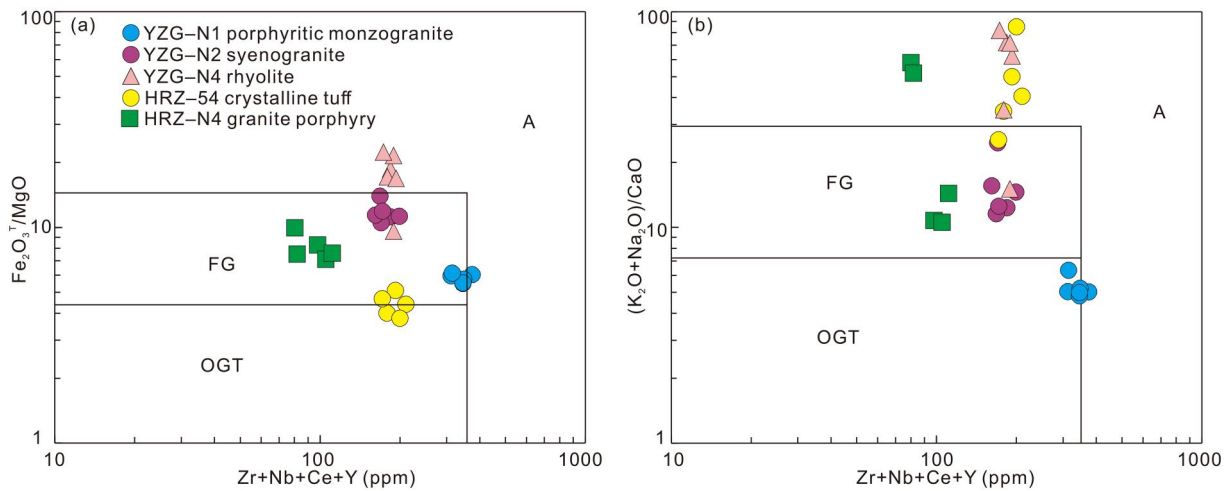


Figure 8. (a) $\text{Fe}_2\text{O}_3^{\text{T}}/\text{MgO}$ vs $\text{Zr} + \text{Nb} + \text{Ce} + \text{Y}$ and (b) $(\text{K}_2\text{O} + \text{Na}_2\text{O})/\text{CaO}$ vs $\text{Zr} + \text{Nb} + \text{Ce} + \text{Y}$ (Whalen *et al.*, 1987). FG, fractionated granite; OGT, unfractionated M-, I-, and S-type granite.

Mg# values (40–42) and low Sr/Y ratios (20–25) characteristic of the trachyandesite. Furthermore, the moderate–high SiO_2 contents (60.29–61.03 wt%) also suggest a crustal affinity rather than a mantle-derived magma. The rock types in the Yazigou area are mainly granite, tuff and rhyolite, and there are no large-scale basaltic magmatic rocks (Figure 2a), indicating that the samples were not formed by AFC of basaltic magma. The AFC will exclude plagioclase and result in an large Eu anomaly, which is contradicted by the weak Eu anomaly ($\text{Eu}/\text{Eu}^* = 0.78\text{--}0.84$) of the trachyandesite. Samples have low mantle compatible element values (*e.g.* Co: 10.34–12.62 ppm; Ni: 5.64–11.19 ppm), which is more like the composition of crust than mantle. Partial melting of the lower crust will produce low Mg# (<45; Rapp *et al.*, 1999; Rapp & Watson, 1995), which is consistent with the trachyandesite. The Lu/Yb (0.156–0.16), Nb/U (3.36–4.16) and Ce/Pb (2.38–3.60) ratios also support an origin from the partial melting of lower crust (Rudnick & Gao, 2003; Sun & McDonough, 1989). Trachyandesite has old $T_{\text{DM}2}$ ages (1330–1217 Ma), suggesting that it was formed by the partial melting of a Mesoproterozoic lower crust. In addition, their $\epsilon_{\text{Hf}}(\text{t})$ contents (–1.08 to 0.7) indicate that only minor mantle material might have been added into their source.

Granite porphyry and crystalline tuff

Granite porphyry and crystalline tuff samples from the Harizha area have high SiO_2 (74.66–78.52 wt%), low $\text{Zr} + \text{Nb} + \text{Ce} + \text{Y}$ values (80–211 ppm), low 10 000 Ga/Al ratios (1.18–2.82) and low T_{Zr} (734–789 °C) (Watson & Harrison, 1983), indicating that they are neither A- nor S- type granites. Samples have low $\text{Fe}_2\text{O}_3^{\text{T}}/\text{MgO}$ and moderate–high $(\text{K}_2\text{O} + \text{Na}_2\text{O})/\text{CaO}$ ratios, showing a signature transitional from I-type to A-type.

There are no contemporaneous large-scale mafic rocks in the Harizha area (Figure 2b), indicating that they were not derived from the differentiation of magma sourced from the mantle. Their Nb/U (1.94–3.81), Ce/Pb (0.3–3.18)

and Rb/Sr (3.65–21.41) ratios suggest that they were related to the crust rather than the mantle. Granite porphyry has negative low $\epsilon_{\text{Hf}}(\text{t})$ values (–7.04 to –5.12) and old $T_{\text{DM}2}$ ages (1703–1581 Ma). In addition, Fan *et al.* (2022) reported that the Harizha crystalline tuff (225 Ma) has $\epsilon_{\text{Hf}}(\text{t})$ values between –8.87 and –2.31 and $T_{\text{DM}2}$ ages between 1820 and 1406 Ma. The age and location of this rock are similar to the crystalline tuff of this study. Thus, we propose that the Harizha granite porphyry and crystalline tuff originated from the partial melting of a Paleo–Mesoproterozoic crust without the addition of mantle material.

Rhyolite

Rhyolite samples have high SiO_2 contents (77.08–79.56 wt%) and low mantle compatible element values (*e.g.* Co: 1.65–2.37 ppm; Ni: 6.18–15.59 ppm), showing that they are not M-type. Samples have high $\text{Fe}_2\text{O}_3^{\text{T}}/\text{MgO}$ and $(\text{K}_2\text{O} + \text{Na}_2\text{O})/\text{CaO}$ ratios, which are consistent with the characteristics of A-type granite (Figure 8a, b). However, it also has low 10 000 Ga/Al ratios (1.67–2.23) and a low T_{Zr} (754–772 °C) (Watson & Harrison, 1983), which are consistent with an I-type granite. Therefore, it may be transitional between I- and A-type. Their Nb/U (1.41–2.64), Ce/Pb (1.82–2.14) and Rb/Sr (3.63–5.43) ratios imply that they were derived from the crust. Based on their $T_{\text{DM}2}$ age (1332–1123 Ma), we propose that it originated from the partial melting of a Mesoproterozoic crust. The $\epsilon_{\text{Hf}}(\text{t})$ contents (–1.31 to 2.01) suggest that there was an injection of mantle material into the source.

Geodynamic evolution

Opening of the Paleo-Tethys Ocean is constrained to the Early Carboniferous by ages of the Haerguole ophiolites (323 Ma) and Derni ophiolites (345–308 Ma; Liu *et al.*, 2011; Yang *et al.*, 2004). Liu *et al.* (2014) reported that initial subduction of the Paleo-Tethys Ocean began at 278 Ma based on a study of the Xiaomiao mafic dyke swarm. Subsequently,

rocks associated with subduction were reported increasingly in the EKOB, such as the Jiadang gabbro (262 Ma; Kong *et al.*, 2017), Wulonggou granodiorite (260 Ma; Luo *et al.*, 2015), Naxiguole gabbro and gabbrodiorite (255–252 Ma; Sun *et al.*, 2021), Shuizhadonggou appinite (248 Ma; Xin *et al.*, 2019) and Xiangride quartz diorite (243 Ma; Xiong *et al.*, 2014). Although the timing of closure of the Paleo-Tethys Ocean is still debated, it is generally considered to have closed prior to the Late Triassic (*e.g.* Xin *et al.*, 2019; Xiong *et al.*, 2014). The angular unconformity between the Middle Triassic Naocanjiangou Formation and the overlying Xilikete Formation supports this conclusion (Chen, 2014). Many extensional-related igneous rocks (*e.g.* Langmaitan A-type granite, 232 Ma; Li *et al.*, 2021) appeared in the EKOB during the Late Triassic, indicating that it was undergoing post-collisional extension at this time. We have collected previously published high-quality geochronological and geochemical data to establish the specific dynamic evolution of the EKOB during the Late Triassic.

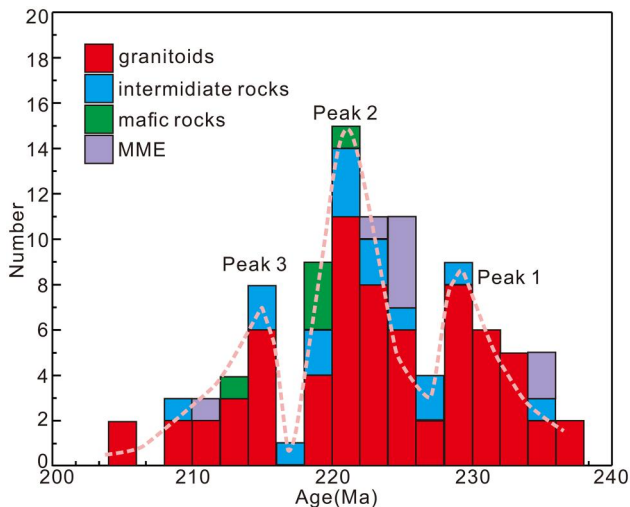


Figure 9. Histogram of zircon U–Pb ages of the Late Triassic magmatism in the EKOB.

The age histogram of Late Triassic igneous rocks in the EKOB reveals three stages of magmatism (Figure 9): stage 1 (S1; 236–227 Ma), stage 2 (S2; 226–218 Ma) and stage 3 (S3; 216–208 Ma). The three stages of magmatism may correspond to different dynamic settings. Post-collision occurs mostly at the end of orogenic cycle, marking the final orogenesis and magmatic activity in the orogenic belt. Magmatism during the period is generally associated with the collapse and extension of the orogenic belt, such as slab break-off and delamination of the lithospheric mantle or lower crust (Rey *et al.*, 2001; Zhou *et al.*, 2021).

In this study, the trachyandesite, porphyritic monzogranite and syenogranite of S1 were formed in the continental crust source with little input of mantle material. Some igneous rocks with MMEs have been reported in this period in the EKOB, such as the Hutouya granodiorite (235 Ma; Feng *et al.*, 2011) and Weibao granodiorite (228 Ma; Zhou *et al.*, 2015). These examples suggest an asthenospheric upwelling during this stage. Based on the Sr/Y and (La/Yb)_N ratios (Figure 10), the crust was still in the process of thickening, so we infer that asthenospheric upwelling was caused by slab break-off rather than delamination, which is one of the common driving forces of magmatism in the early stage of post-collisional extension (Yan *et al.*, 2022). In fact, some magmatic rocks associated with slab break-off have been reported, such as the Elashan quartz monzodiorite (236 Ma; Wu *et al.*, 2021) and Tuoketuo granodiorite (232 Ma; Xia, Qing, *et al.*, 2014). Therefore, we propose that the asthenospheric upwelling caused by the slab break-off provided heat for the partial melting of lithospheric mantle during S1. The rising of hot lithospheric mantle melt resulted in the partial melting of a Mesoproterozoic crust in the EKOB, and only minor mantle material was added to the crustal melt, producing various types of rocks during the process (Figure 11a).

Previously published data have shown the appearance of large amounts of adakitic rocks during S2, such as the Xilikete granodiorite (225 Ma; Chen *et al.*, 2013), Xiangride porphyritic granodiorite (223 Ma; Xiong *et al.*, 2014) and

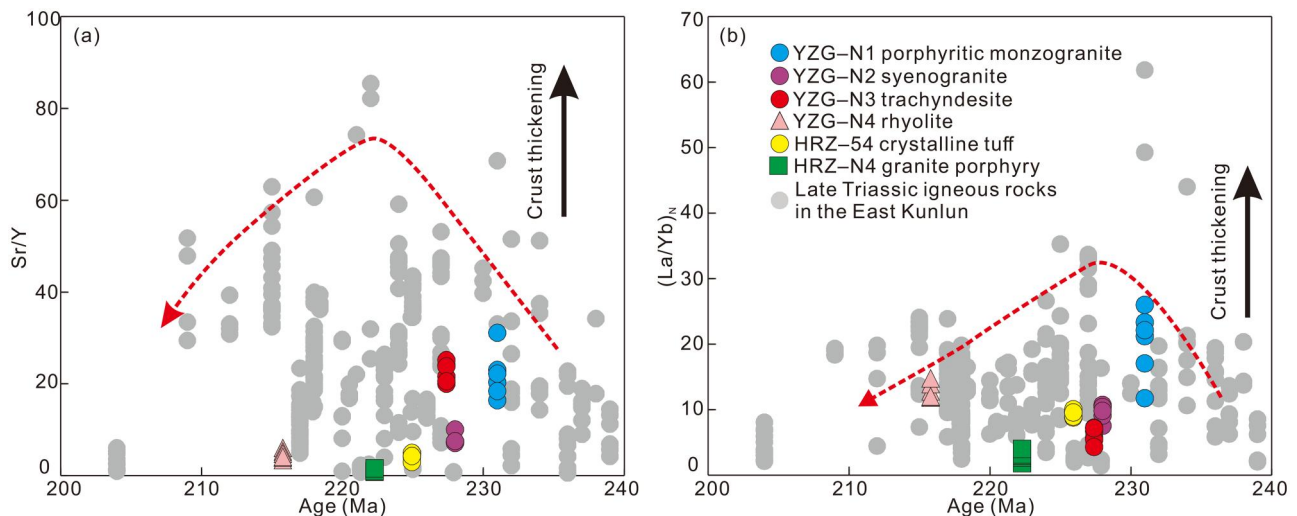


Figure 10. (a) Sr/Y vs age and (b) (La/Yb)_N vs age for the Late Triassic rocks from the EKOB.

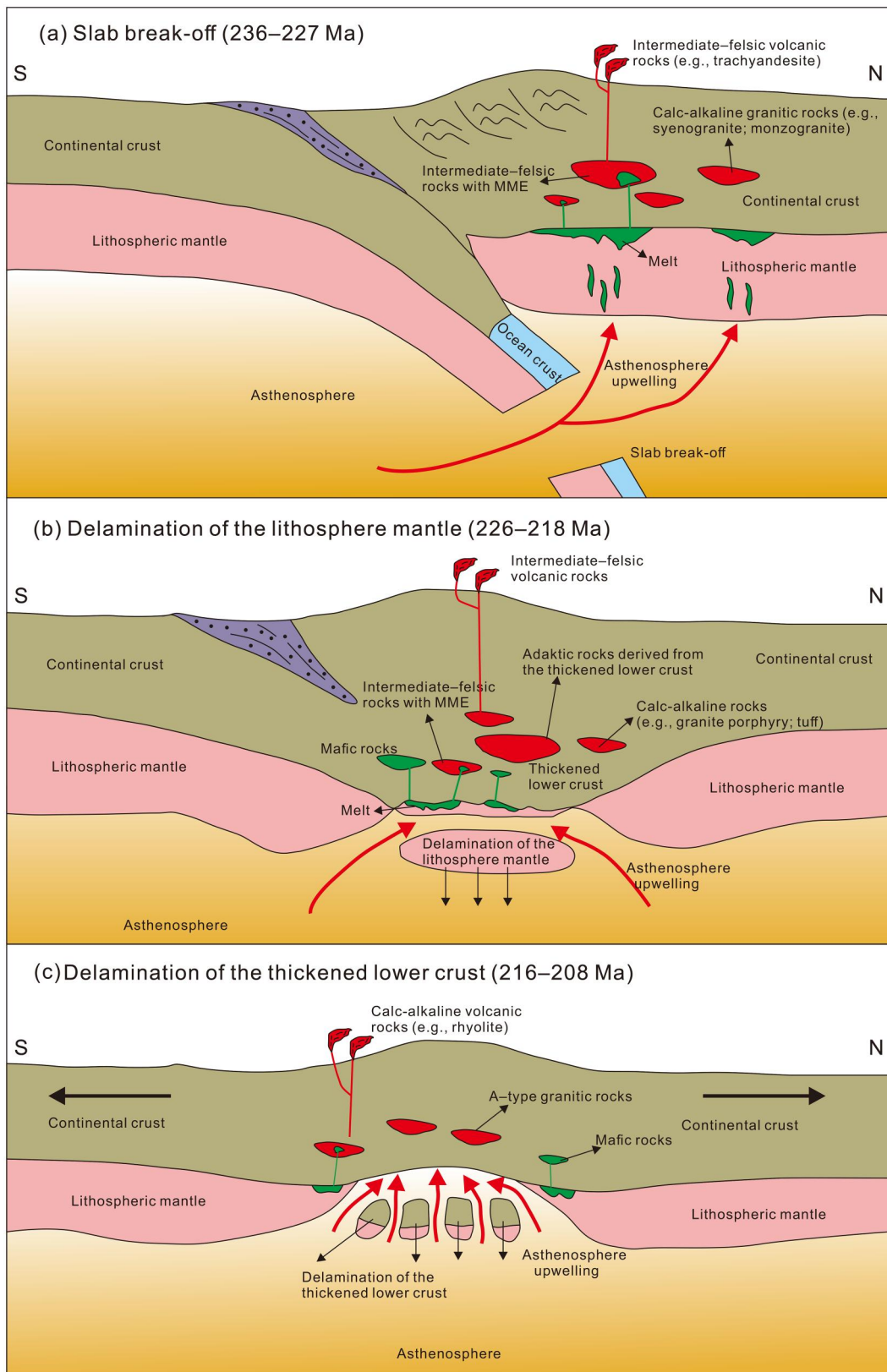


Figure 11. Schematic diagram showing a genetic model for the Late Triassic igneous rocks in the EKOB.

Xiao-Nuomuhong granodiorite (222 Ma; Xia, Wang, *et al.*, 2014). In addition, some igneous rocks are also characterised by high Sr/Y and $(La/Yb)_N$ ratios during this period

(Figure 10), suggesting that there was a thickened crust in the EKOB at this time. Moreover, Luo (2012) reported an uplift event in the EKOB triggered by extrusion related to

the closure of the Paleo-Tethys Ocean. Xia, Wang, *et al.* (2014) and Xia, Qing, *et al.* (2014) reported that there was approximately 35 km crust beneath the EKOB at about 222 Ma. All geochemical data confirm a thickened crust beneath the EKOB. There are mafic rocks and granitic rocks with MMEs (Figure 9), implying that the delamination occurred at this stage. Studies have shown that the thickened crust cannot sink directly because of the refractory and buoyant nature of the underlying lithospheric mantle (Deng *et al.*, 2007), so the lithospheric mantle delamination is the best explanation for the genesis of igneous rocks in this interval. Asthenospheric upwelling caused by delamination heated the thickened lower thickened crust to produce adakitic rocks and granitic rocks, and some mantle material rose directly to the crust to form mafic rocks or was added to felsic magmas in the form of MMEs (Figure 11b).

The Sr/Y and (La/Yb)_N ratios of igneous rocks in the S3 interval were decreasing (Figure 10), indicating that the crust was in the process of thinning. The occurrence of intrusive rocks (*e.g.* Yemaquan syenogranite; 213 Ma; Gao *et al.*, 2014) and volcanic rocks (*e.g.* Xiangride rhyolite; 213 Ma; Ding *et al.*, 2011) with the characteristics of A-type granite indicate also that the EKOB was undergoing extensional magmatism during the S3 interval. In addition, Zhao *et al.* (2020) reported that the Kengdenongshe granite porphyry (211 Ma) was associated with asthenospheric upwelling in the EKOB. We infer that the extensional magmatism was probably caused by asthenospheric upwelling triggered by delamination of the thickened lower crust. Previous studies have shown that the subsequent collision will cause the crust to continue to thicken, forming the lower crust of eclogite facies (Chiaradia *et al.*, 2009; Kapp *et al.*, 2008). The increase in density results in the change in its stability, and the upwelling of asthenosphere caused by lithospheric delamination further changes the physical properties of the thickened crust. Under the influence of various processes, the thickened lower crust of eclogite facies delaminated, leading to the extensional magmatism in the EKOB (Figure 11c).

Conclusions

The intermediate–felsic igneous rocks from the Yazigou and Harizha areas were formed at 231.1–215.8 Ma (*i.e.* Late Triassic). The porphyritic monzogranite (231.1 Ma), syenogranite (228.1 Ma), trachyandesite (227.4 Ma) and rhyolite (215.8 Ma) were formed by the partial melting of a Mesoproterozoic crust with only minor input of mantle material into their source. Crystalline tuff (224.6 Ma) and granite porphyry (222.3 Ma) were derived from the partial melting of a Paleo–Mesoproterozoic crust without the addition of mantle material. We identify three intervals of magmatism (S1: 236–227 Ma; S2: 226–218 Ma; S3: 216–208 Ma) in the post-collisional stage of the EKOB, and they

correspond to slab break-off, lithospheric mantle delamination and the thickened lower crust delamination, respectively.

Funding

This research was funded by the Key Research Program of the National Natural Science Foundation of China (92062217), the Kunlun Talents High-end Innovative and Entrepreneurial Talents Project of Qinghai Province ([2022] No. 32), the Science and Technology Project of Qinghai Province (2019-ZJ-7009) and the Kunlun Talents High-end Innovative and Entrepreneurial Talents Project of Qinghai Province ([2021] No. 16).

Data availability statement

The authors confirm that the data supporting the findings of this study are available within the article and the [Supplemental data](#).

Disclosure statement

No potential conflict of interest was reported by the author(s).

References

- Alirezai, S., & Cameron, E. M. (2002). Mass balance during gabbro–amphibolite transition, Bamble Sector, Norway: Implications for petrogenesis and tectonic setting of the gabbros. *Lithos*, 60(1–2), 21–45. [https://doi.org/10.1016/S0024-4937\(01\)00076-7](https://doi.org/10.1016/S0024-4937(01)00076-7)
- Andersen, T. (2002). Correction of common lead in U–Pb analyses that do not report ²⁰⁴Pb. *Chemical Geology*, 192(1–2), 59–79. [https://doi.org/10.1016/S0009-2541\(02\)00195-x](https://doi.org/10.1016/S0009-2541(02)00195-x)
- Bellos, L. I., Castro, A., Díaz-Alvarado, J., & Toselli, A. (2015). Multi-pulse cotectic evolution and in-situ fractionation of calc-alkaline tonalite–granodiorite rocks, Sierra de Velasco batholith, Famatinian belt, Argentina. *Gondwana Research*, 27(1), 258–280. <https://doi.org/10.1016/j.gr.2013.09.019>
- Bonin, B. (2004). Do coeval mafic and felsic magmas in post-collisional to within-plate regimes necessarily imply two contrasting, mantle and crustal, sources? A review. *Lithos*, 78(1–2), 1–24. <https://doi.org/10.1016/j.lithos.2004.04.042>
- Boynton, W. V. (1984). Geochemistry of the rare earth elements: Meteorite studies. In P. Henderson (Ed.), *Rare earth element geochemistry* (pp. 63–114). Elsevier.
- Carmichael, I. S. E. (2002). The andesite aqueduct: Perspectives on the evolution of intermediate magmatism in west-central (105–99°W) Mexico. *Contributions to Mineralogy and Petrology*, 143(6), 641–663. <https://doi.org/10.1007/s00410-002-0370-9>
- Champion, D. C., & Chappell, B. W. (1992). Petrogenesis of felsic I-type granites: An example from northern Queensland. *Earth and Environmental Science Transactions of the Royal Society of Edinburgh*, 83(1–2), 115–126. <https://doi.org/10.1017/S026359330000780>
- Chappell, B. W. (1999). Aluminium saturation in I- and S-type granites and the characterization of fractionated haplogranites. *Lithos*, 46(3), 535–551. [https://doi.org/10.1016/S0024-4937\(98\)00086-3](https://doi.org/10.1016/S0024-4937(98)00086-3)
- Chen, E. N. (2014). *Geologic features, provenance analysis and structural evolution of Naocangjiangou formation at the in the southern slope of the East Kunlun (East part)* [Unpublished master's thesis]. Chang'an University (in Chinese).
- Chen, G. C., Pei, X. Z., Li, R. B., Li, Z. C., Pei, L., Liu, C. J., Chen, Y. X., Wang, M., Gao, F., & Li, X. B. (2019). Lithospheric extension of the post-collision stage of the Paleo-Tethys oceanic system in the East Kunlun Orogenic Belt: Insights from Late Triassic plutons. *Earth*

- Science Frontiers*, 26(4), 191–208. <https://doi.org/10.13745/j.esf.sf.2019.1.18>
- Chen, G. C., Pei, X. Z., Li, R. B., Li, Z. C., Pei, L., Liu, Z. Q., Chen, Y. X., & Liu, C. J. (2013). Late Triassic magma mixing in the East Kunlun orogenic belt: A case study of Helegang Xilikete granodiorites. *Geology in China*, 40(4), 1044–1065 (in Chinese).
- Chen, L., Sun, Y., Pei, X. Z., Gao, M., Tao, F., Zhang, Z. Q., & Chen, W. (2001). Northernmost Paleo-Tethyan oceanic basin in Tibet: Geochronological evidence from ^{40}Ar – ^{39}Ar age dating of Dur'ngoi ophiolite. *Chinese Science Bulletin*, 46(14), 1203–1205. <https://doi.org/10.1007/BF02900603>
- Chen, L., & Zhao, Z. F. (2017). Origin of continental arc andesites: The composition of source rocks is the key. *Journal of Asian Earth Sciences*, 145, 217–232. <https://doi.org/10.1016/j.jseae.2017.04.012>
- Chen, N. S., Li, X. Y., Zhang, K. X., Wang, G. C., Zhu, Y. H., Hou, G. J., & Bai, Y. S. (2006). Lithological characteristics of the Baishahe Formation to the south of Xiangride Town, Eastern Kunlun Mountains and its age constrained from zircon U–Pb dating. *Geological Science Technology Information*, 25, 1–7 (in Chinese with English abstract).
- Chiaradia, M., Müntener, O., Beate, B., & Fontignie, D. (2009). Adakite-like volcanism of Ecuador: Lower crust magmatic evolution and recycling. *Contributions to Mineralogy and Petrology*, 158(5), 563–588. <https://doi.org/10.1007/s00410-009-0397-2>
- Deng, J., Su, S., Niu, Y., Liu, C., Zhao, G., Zhao, X., Zhou, S., & Wu, Z. (2007). A possible model for the lithospheric thinning of North China Craton: Evidence from the Yanshanian (Jura-Cretaceous) magmatism and tectonism. *Lithos*, 96(1–2), 22–35. <https://doi.org/10.1016/j.lithos.2006.09.009>
- Ding, Q. F., Jiang, S. Y., & Sun, F. Y. (2014). Zircon U–Pb geochronology, geochemical and Sr–Nd–Hf isotopic compositions of the Triassic granite and diorite dikes from the Wulonggou mining area in the Eastern Kunlun Orogen, NW China: Petrogenesis and tectonic implications. *Lithos*, 205, 266–283. <https://doi.org/10.1016/j.lithos.2014.07.015>
- Ding, S., Huang, H., Niu, Y. L., Zhao, Z. D., Yu, X. H., & Mo, X. X. (2011). Geochemistry, geochronology and petrogenesis of East Kunlun high Nb–Ta rhyolites. *Acta Petrologica Sinica*, 27(12), 3603–3614 (in Chinese).
- Eby, G. N. (1992). Chemical subdivision of the A-type granitoids: Petrogenetic and tectonic implications. *Geology*, 20(7), 641–644. [https://doi.org/10.1130/0091-7613\(1992\)020<0641:CSOTAT>2.3.CO;2](https://doi.org/10.1130/0091-7613(1992)020<0641:CSOTAT>2.3.CO;2)
- Fan, X., Sun, F., Xu, C., Wu, D., Yu, L., Wang, L., Yan, C., & Bakht, S. (2022). Volcanic rocks of the Elashan Formation in the Dulan-Xiangride Basin, East Kunlun Orogenic Belt, NW China: Petrogenesis and implications for Late Triassic geodynamic evolution. *International Geology Review*, 64(9), 1270–1293. <https://doi.org/10.1080/00206814.2021.1923074>
- Feng, Y. C., Wang, X. P., Shu, X. F., Zhang, A. K., Xiao, Y., Liu, J. N., Ma, S. C., Li, C. G., & Li, D. X. (2011). Isotopic chronology of the Hutouya skarn lead–zinc polymetallic ore district in Qimantage area of Qinghai Province and its geological significance. *Journal of Jilin University*, 41(6), 1806–1817 (in Chinese).
- Fliedert, T. V. D., Hoernes, S., Jung, S., Masberg, P., Hoffer, E., Schaltegger, U., & Friedrichsen, H. (2003). Lower crustal melting and the role of open-system processes in the genesis of syn-orogenic quartz diorite–granite–leucogranite associations: Constraints from Sr–Nd–O isotopes from the Bandombaai complex, Namibia. *Lithos*, 67(3–4), 205–226. [https://doi.org/10.1016/S0024-4937\(03\)00016-1](https://doi.org/10.1016/S0024-4937(03)00016-1)
- Gao, P., Zheng, Y. F., & Zhao, Z. F. (2016). Experimental melts from crustal rocks: A lithochemical constraint on granite petrogenesis. *Lithos*, 266–267, 133–157. <https://doi.org/10.1016/j.lithos.2016.10.005>
- Gao, Y. B., Li, W. Y., Qian, B., Li, K., Li, D. S., He, S. Y., Zhang, Z. W., & Zhang, J. W. (2014). Geochronology, geochemistry and Hf isotopic compositions of the granitic rocks related with iron mineralization in Yemaquan deposit, East Kunlun, NW China. *Acta Petrologica Sinica*, 30(6), 1647–1665. (in Chinese).
- Goolaerts, A., Mattielli, N., de Jong, J., Weis, D., & Scoates, J. S. (2004). Hf and Lu isotopic reference values for the zircon standard 91500 by MC-ICP-MS. *Chemical Geology*, 206(1–2), 1–9. <https://doi.org/10.1016/j.chemgeo.2004.01.008>
- Guffanti, M., Clynne, M. A., & Muffler, L. J. P. (1996). Thermal and mass implications of magmatic evolution in the Lassen volcanic region, California, and minimum constraints on basalt influx to the lower crust. *Journal of Geophysical Research: Solid Earth*, 101(B2), 3003–3013. <https://doi.org/10.1029/95JB03463>
- Guo, F., Nakamura, E., Fan, W. M., Kobayoshi, K., & Li, C. W. (2007). Generation of Palaeocene adakitic andesites by magma mixing in Yanji area, NE China. *Journal of Petrology*, 48(4), 661–692. <https://doi.org/10.1093/petrology/egl077>
- Hofmann, A. W., Jochum, K. P., Seufert, M., & White, W. M. (1986). Nb and Pb in oceanic basalts: New constraints on mantle evolution. *Earth and Planetary Science Letters*, 79(1–2), 33–45. [https://doi.org/10.1016/0012-821X\(86\)90038-5](https://doi.org/10.1016/0012-821X(86)90038-5)
- Hoskin, P. W. O., & Schaltegger, U. (2003). The composition of zircon and igneous and metamorphic petrogenesis. *Reviews in Mineralogy and Geochemistry*, 53(1), 27–62. <https://doi.org/10.2113/0530027>
- Hu, Y., Niu, Y. L., Li, J. Y., Ye, L., Kong, J. J., Chen, S., Zhang, Y., & Zhang, G. R. (2016). Petrogenesis and tectonic significance of the Late Triassic mafic dikes and felsic volcanic rocks in the East Kunlun Orogenic Belt, Northern Tibet Plateau. *Lithos*, 245, 205–222. <https://doi.org/10.1016/j.lithos.2015.05.004>
- Irvine, T. N., & Baragar, W. R. A. (1971). A guide to the chemical classification of the common volcanic rocks. *Canadian Journal of Earth Sciences*, 8(5), 523–548. <https://doi.org/10.1139/e71-055>
- Ji, Z., Ge, W. C., Yang, H., Bi, J. H., Yu, Q., & Dong, Y. (2018). The Late Triassic Andean-type andesite from the central Great Xing'an range: Products of the southward subduction of the Mongol-Okhotsk oceanic plate. *Acta Petrologica Sinica*, 34(10), 2917–2930 (in Chinese).
- Kapp, P., Taylor, M., Stockli, D., & Ding, L. (2008). Development of active low-angle normal fault systems during orogenic collapse: Insight from Tibet. *Geology*, 36(1), 7–10. <https://doi.org/10.1130/G24054A.1>
- Kong, H. L., Li, J. C., Li, Y. Z., Jia, Q. Z., & Guo, X. Z. (2017). Zircon LA-ICP-MS U–Pb dating and its geological significance of the Jiadang gabbro in the eastern section of East Kunlun, Qinghai Province. *Geology and Exploration*, 53(5), 889–902 (in Chinese). <https://doi.org/10.13712/j.cnki.dzykt.2017.05.006>
- Lee, C. T. A., Lee, T. C., & Wu, C. T. (2014). Modeling the compositional evolution of recharging, evacuating, and fractionating (REFC) magma chambers: Implications for differentiation of arc magmas. *Geochimica et Cosmochimica Acta*, 143, 8–22. <https://doi.org/10.1016/j.gca.2013.08.009>
- Li, J. C., Xian, G. Z., Kong, H. L., Yao, X. G., & Jia, Q. Z. (2021). Geochronology, geochemical characteristics, and geological significance of A-type granite from the Langmaitan area, East Kunlun. *Acta Geological Sinica*, 95(5), 1508–1522 (in Chinese).
- Li, R. B., Pei, X. Z., Li, Z. C., Pei, L., Chen, G. C., Chen, Y. X., Liu, C. J., & Wang, S. M. (2018). Paleo-Tethys Ocean subduction in eastern section of East Kunlun Orogen: Evidence from the geochronology and geochemistry of the Wutuo pluton. *Acta Petrologica Sinica*, 34(11), 3399–3421 (in Chinese).
- Liu, B., Ma, C. Q., Zhang, J. Y., Xiong, F. H., Huang, J., & Jiang, H. A. (2014). ^{40}Ar – ^{39}Ar age and geochemistry of subduction-related mafic dikes in northern Tibet, China: Petrogenesis and tectonic implications. *International Geology Review*, 56(1), 57–73. <https://doi.org/10.1080/00206814.2013.818804>
- Liu, Y., Hu, Z., Gao, S., Günther, D., Xu, J., Gao, C., & Chen, H. (2008). In situ analysis of major and trace elements of anhydrous minerals by LA-ICP-MS without applying an internal standard. *Chemical Geology*, 257(1–2), 34–43. <https://doi.org/10.1016/j.chemgeo.2008.08.004>
- Liu, Z. Q., Pei, X. Z., Li, R. B., Li, Z. C., Zhang, X. F., Liu, Z. G., Chen, G. C., Chen, Y. X., Ding, S. P., & Guo, J. F. (2011). LA-ICP-MS zircon U–Pb geochronology of the two suites of ophiolites at the

- Buqingshan Area of the A'nyemaqen Orogenic Belt in the southern margin of East Kunlun and its tectonic implication. *Acta Geological Sinica*, 85, 185–194 (in Chinese).
- Ludwig, K. R. (2003). *ISOPLOT 3.00: A Geochronological Toolkit for Microsoft Excel*. Berkeley Geochronology Center, California.
- Luo, M., Mo, X., Yu, X., Li, X., & Huang, X. (2015). Zircon U–Pb geochronology, petrogenesis and implication of the Later Permian granodiorite from the Wulonggou Area in East Kunlun, Qinhai Province. *Earth Science Frontiers*, 22(5), 182–195. <https://doi.org/10.13745/j.esf.2015.05.015>
- Luo, M. F., Mo, X. X., Yu, X. H., Li, X. W., Huang, X. F., & Yu, J. C. (2014). Zircon LA-ICP-MS U–Pb age dating, petrogenesis and tectonic implications of the Late Triassic granites from the Xiangride area, East Kunlun. *Acta Petrologica Sinica*, 30(11), 3229–3241 (in Chinese).
- Luo, W. X. (2012). *Petrogenesis and tectono-thermal history of the plutonic pyroxenite in the middle of East Kunlun orogen, western China* [unpublished doctoral thesis]. China University of Geoscience, 136 pp. (in Chinese).
- Mo, X. X., Luo, Z. H., Deng, J. F., Yu, X. H., Liu, C. D., Chen, H. W., Yuan, W. M., & Liu, Y. H. (2007). Granitoids and crustal growth in the East-Kunlun Orogenic Belt. *Geology Journal of China University*, 13, 403–414 (in Chinese).
- Peccerillo, A., & Taylor, S. R. (1976). Geochemistry of Eocene calc-alkaline volcanic rocks from the Kastamonu area, northern Turkey. *Contributions to Mineralogy and Petrology*, 58(1), 63–81. <https://doi.org/10.1007/BF00384745>
- Rapp, R. P., Shimizu, N., Norman, M. D., & Applegate, G. S. (1999). Reaction between slab-derived melts and peridotite in the mantle wedge: Experimental constraints at 3.8 GPa. *Chemical Geology*, 160(4), 335–356. [https://doi.org/10.1016/S0009-2541\(99\)00106-0](https://doi.org/10.1016/S0009-2541(99)00106-0)
- Rapp, R. P., & Watson, E. B. (1995). Dehydration melting of meta basalt at 8–32 kbar: Implications for continental growth and crust–mantle recycling. *Journal of Petrology*, 36(4), 891–931. <https://doi.org/10.1093/ptrology/36.4.891>
- Reubi, O., & Blundy, J. (2009). A dearth of intermediate melts at subduction zone volcanoes and the petrogenesis of arc andesites. *Nature*, 461(7268), 1269–1273. <https://doi.org/10.1038/nature08510>
- Rey, P., Vanderhaeghe, O., & Teyssier, C. (2001). Gravitational collapse of the continental crust: Definition, regimes, and modes. *Tectonophysics*, 342(3–4), 435–449. [https://doi.org/10.1016/S0040-1951\(01\)00174-3](https://doi.org/10.1016/S0040-1951(01)00174-3)
- Richards, J. P. (2011). Magmatic to hydrothermal metal fluxes in convergent and collided margins. *Ore Geology Reviews*, 40(1), 1–26. <https://doi.org/10.1016/j.oregeorev.2011.05.006>
- Roger, F., Arnaud, N., Gilder, S., Tapponnier, P., Jolivet, M., Brunel, M., Malavieille, J., Xu, Z. Q., & Yang, J. S. (2003). Geochronological and geochemical constraints on Mesozoic suturing in east central Tibet. *Tectonics*, 22(4), 1037. <https://doi.org/10.1029/2002TC001466>
- Rudnick, R. L., & Gao, S. (2003). Composition of the continental crust. In H. D. Holland & K. K. Turekian (Eds.), *Treatise on geochemistry* (Vol. 3, 2nd ed., pp. 1–66). Elsevier Science. <https://doi.org/10.1016/B978-0-08-095975-7.00301-6>
- Rudnick, R. L., McLennan, S. M., & Taylor, S. R. (1985). Large ion lithophile elements in rocks from high-pressure granulite facies terranes. *Geochimica et Cosmochimica Acta*, 49(7), 1645–1655. [https://doi.org/10.1016/0016-7037\(85\)90268-6](https://doi.org/10.1016/0016-7037(85)90268-6)
- Sengör, A. M. (1979). Mid-Mesozoic closure of Permo-Triassic Tethys and its implications. *Nature*, 279, 590–593. <https://doi.org/10.1038/279590a0>
- Sun, F. Y., Li, B. L., Ding, Q. F., Zhao, J. W., Pan, T., Yu, X. F., Wang, L., Chen, G. J., & Ding, Z. J. (2009). *Research on the key problems of ore prospecting in the Eastern Kunlun metallogenic belt*. Geological Survey Institute of Jilin University (in Chinese).
- Sun, J. L., Qian, Y., Li, Y. J., Li, H. R., Tian, S. N., & Sun, F. Y. (2021). Intermittent subduction of the Paleo-Tethys Ocean in the middle-late Permian: Evidence from the mafic–intermediate intrusive rocks in the East Kunlun Orogenic Belt. *Australian Journal of Earth Sciences*, 68(2), 229–244. <https://doi.org/10.1080/08120099.2020.1764623>
- Sun, S. S., & McDonough, W. F. (1989). Chemical and isotopic systematics of oceanic basalts: Implications for mantle composition and processes. *Geological Society, London, Special Publications*, 42(1), 313–345. <https://doi.org/10.1144/GSL.SP.1989.042.01.19>
- Turner, S. P., Foden, J. D., & Morrison, R. S. (1992). Derivation of some A-type magmas by fractionation of basaltic magma: An example from the Padthaway Ridge, South Australia. *Lithos*, 28(2), 151–179. [https://doi.org/10.1016/0024-4937\(92\)90029-X](https://doi.org/10.1016/0024-4937(92)90029-X)
- Wang, G. C., Wei, Q. R., Jia, C. X., Zhang, K. X., Li, D. W., Zhu, Y. H., & Xiang, S. Y. (2007). Some ideas of Precambrian geology in the East Kunlun. *Geological Bulletin of China*, 26, 929–937 (in Chinese with English abstract).
- Watson, E. B., & Harrison, T. M. (1983). Zircon saturation revisited: Temperature and composition effects in a variety of crustal magma types. *Earth and Planetary Science Letters*, 64(2), 295–304. [https://doi.org/10.1016/0012-821X\(83\)90211-X](https://doi.org/10.1016/0012-821X(83)90211-X)
- Whalen, J. B., Currie, K. L., & Chappell, B. W. (1987). A-type granites: Geochemical characteristics, discrimination and petrogenesis. *Contributions to Mineralogy and Petrology*, 95(4), 407–419. <https://doi.org/10.1007/BF00402202>
- Wiedenbeck, M., Allé, P., Corfu, F., Griffin, W. L., Meier, M., Oberli, F., Quadt, A. V., Roddick, J. C., & Spiegel, W. (1995). Three natural zircon standards for U–Th–Pb, Lu–Hf, trace element and REE analyses. *Geostandards and Geoanalytical Research*, 19(1), 1–23. <https://doi.org/10.1111/j.1751-908X.1995.tb00147.x>
- Windley, B. F., Alexeiev, D., Xiao, W., Kröner, A., & Badarch, G. (2007). Tectonic models for accretion of the Central Asian Orogenic Belt. *Journal of the Geological Society*, 164(1), 31–47. <https://doi.org/10.1144/0016-76492006-022>
- Wu, D. Q., Sun, F. Y., Pan, Z. C., & Tian, N. (2021). Geochronology, geochemistry, and Hf isotopic compositions of Triassic igneous rocks in the easternmost segment of the East Kunlun Orogenic Belt, NW China: Implications for magmatism and tectonic evolution. *International Geology Review*, 63(8), 1011–1029. <https://doi.org/10.1080/00206814.2020.1740895>
- Wu, F. Y., Yang, Y. H., Xie, L. W., Yang, J. H., & Xu, P. (2006). Hf isotopic compositions of the standard zircons and baddeleyites used in U–Pb geochronology. *Chemical Geology*, 234(1–2), 105–126. <https://doi.org/10.1016/j.chemgeo.2006.05.003>
- Xia, R., Qing, M., Wang, C. M., & Li, W. L. (2014). The genesis of the ore-bearing porphyry of the Tuoketuo porphyry Cu–Au (Mo) deposit in the East Kunlun, Qinghai Province: Constraints from zircon U–Pb geochronological and geochemistry. *Journal of Jilin University (Earth Science Edition)*, 5, 1502–1524 (in Chinese).
- Xia, R., Wang, C. M., Deng, J., Carranza, E. J. M., Li, W. L., & Qing, M. (2014). Crustal thickening prior to 220 Ma in the East Kunlun Orogenic Belt: Insights from the Late Triassic granitoids in the Xiaonuo-muhong pluton. *Journal of Asian Earth Sciences*, 93, 193–210. <https://doi.org/10.1016/j.jseaes.2014.07.013>
- Xiao, W. J., Windley, B. F., Huang, B. C., Han, C. M., Yuan, C., Chen, H. L., Sun, M., Sun, S., & Li, J. L. (2009). End-Permian to Mid-Triassic termination of the accretionary processes of the southern Altaids: Implications for the geodynamic evolution, Phanerozoic continental growth, and metallogeny of Central Asia. *International Journal of Earth Sciences*, 98(6), 1189–1217. <https://doi.org/10.1007/s00531-008-0407-z>
- Xie, H., Wang, Y., Li, D., Zhou, G., & Zhang, Z. (2021). Late Triassic magma mixing and fractional crystallization in the Qingchengzi Orefield, Eastern Liaoning Province: Regional petrogenetic and metallogenic implications. *Journal of Earth Science*, 32(1), 144–157. <https://doi.org/10.1007/s12583-020-1114-3>
- Xin, W., Sun, F. Y., Zhang, Y. T., Fan, X. Z., Wang, Y. C., & Li, L. (2019). Mafic–intermediate igneous rocks in the East Kunlun Orogenic Belt, northwestern China: Petrogenesis and implications for regional geodynamic evolution during the Triassic. *Lithos*, 346–347, 105159. <https://doi.org/10.1016/j.lithos.2019.105159>

- Xiong, F. H. (2014). *Spatial-temporal pattern, petrogenesis and geological implications of Paleo-Tethyan granitoids in the East Kunlun Orogenic Belt (Eastern Segment)* [Unpublished doctoral dissertation]. China University of Geosciences (in Chinese).
- Xiong, F. H., Ma, C. Q., Zhang, J. Y., & Liu, B. (2011). LA-ICP-MS zircon U–Pb dating, elements and Sr–Nd–Hf isotope geochemistry of the early Mesozoic mafic dyke swarms in East Kunlun orogenic belt. *Acta Petrologica Sinica*, 27(11), 3350–3364. (in Chinese)
- Xiong, F. H., Ma, C. Q., Zhang, J. Y., & Liu, B. (2012). The origin of mafic microgranular enclaves and their host granodiorites from East Kunlun, Northern Qinghai-Tibet Plateau: Implications for magma mixing during subduction of Paleo-Tethyan lithosphere. *Mineralogy and Petrology*, 104(3–4), 211–224. <https://doi.org/10.1007/s00710-011-0187-1>
- Xiong, F. H., Ma, C., Zhang, J., Liu, B., & Jiang, H. (2014). Reworking of old continental lithosphere: An important crustal evolution mechanism in orogenic belts, as evidenced by Triassic I-type granitoids in the East Kunlun orogen, Northern Tibetan Plateau. *Journal of the Geological Society*, 171(6), 847–863. <https://doi.org/10.1144/jgs2013-038>
- Yan, M. Q., Wei, J. H., Zhang, D. H., Zhao, Z. X., Turlin, F., Li, H., Li, G. M., Xu, C. W., Zhang, X. M., & Moritz, R. (2022). Petrogenesis of Late Devonian I- and A-type granitoids, and associated mafic microgranular enclaves in the northwestern North Qaidam Orogenic Belt, China: Implications for continental crust growth during the post-collisional stage. *Lithos*, 430–431, 106857. <https://doi.org/10.1016/j.lithos.2022.106857>
- Yang, J. S., Wang, X. B., Shi, R. D., Xu, Z. Q., & Wu, C. L. (2004). The Dur'ngoi ophiolite in East Kunlun, northern Qinghai-Tibet Plateau: A fragment of Paleo-Tethyan oceanic crust. *Geology in China*, 31, 225–239 (in Chinese).
- Yin, A., & Harrison, T. M. (2000). Geologic evolution of the Himalayan-Tibetan orogen. *Annual Review of Earth and Planetary Sciences*, 28(1), 211–280. <https://doi.org/10.1146/annurev.earth.28.1.211>
- Yu, M., Feng, C. Y., Zhao, Y. M., & Li, D. X. (2015). Genesis of post-collisional calc-alkaline and alkaline granitoids in Qiman Tagh, East Kunlun, China. *Lithos*, 239, 45–59. <https://doi.org/10.1016/j.lithos.2015.08.022>
- Yu, Q., Ge, W. C., Zhang, J., Zhao, G. C., Zhang, Y. L., & Yang, H. (2017). Geochronology, petrogenesis and tectonic implication of Late Paleozoic volcanic rocks from the Dashizhai Formation in Inner Mongolia, NE China. *Gondwana Research*, 43, 164–177. <https://doi.org/10.1016/j.gr.2016.01.010>
- Yuan, C., Zhou, M. F., Sun, M., Zhao, Y., Wilde, S., Long, X., & Yan, D. P. (2010). Triassic granitoids in the eastern Songpan Ganzi Fold Belt, SW China, Magmatic response to geodynamics of the deep Lithosphere. *Earth and Planetary Science Letters*, 290(3–4), 481–492. <https://doi.org/10.1016/j.epsl.2010.01.005>
- Zhao, X., Wei, J., Fu, L., Huizenga, J. M., Santosh, M., Chen, J., Wang, D., & Li, A. (2020). Multi-stage crustal melting from Late Permian back-arc extension through Middle Triassic continental collision to Late Triassic post-collisional extension in the East Kunlun Orogen. *Lithos*, 360–361, 105446. <https://doi.org/10.1016/j.lithos.2020.105446>
- Zhou, C. A., Song, S., Allen, M. B., Wang, C., Su, L., & Wang, M. (2021). Post-collisional mafic magmatism: Insights into orogenic collapse and mantle modification from North Qaidam collisional belt, NW China. *Lithos*, 398–399, 106311. <https://doi.org/10.1016/j.lithos.2021.106311>
- Zhou, J. H., Feng, Y. C., Shen, D. L., Li, D. X., Wang, H., Zhang, M. Y., & Ma, S. C. (2015). Geochronology, geochemistry and tectonic implications of granodiorite in the Northwest of Weibao Deposit, Xinjing Qimantage. *Acta Geological Sinica*, 89(3), 473–486 (in Chinese).